Physics – Uspekhi **46** (4) 393 – 403 (2003)

METHODOLOGICAL NOTES PACS numbers: **05.45. – a**, **45.10. – b**, **45.40. – f**

Strange attractors in rattleback dynamics

A V Borisov, I S Mamaev

DOI: 10.1070/PU2003v046n04ABEH001306

Contents

Abstract. This review is dedicated to the dynamics of the rattleback, a phenomenon with curious physical properties that is studied in nonholonomic mechanics. All known analytical results are collected here, and some results of our numerical simulation are presented. In particular, three-dimensional Poincaré maps associated with dynamical systems are systematically investigated for the first time. It is shown that the loss of stability of periodic and quasiperiodic solutions, which gives rise to strange attractors, is typical of the three-dimensional maps related to rattleback dynamics. This explains some newly discovered properties of the rattleback related to the transition from regular to chaotic solutions at certain values of the physical parameters.

1. Introduction

First we are going to make some physical and historical comments about the rattleback, describe its basic physical properties, and mention investigations on the subject that have already been made. For a preview of what the rattleback is, we recommend an interesting paper by J Walker [1].

The unusual properties of the rattleback's behavior are as follows. When placed on a horizontal surface and spun in a certain direction about the vertical axis, it spins freely; if, however, it is made to rotate in the opposite direction, it soon stops rotating, begins to oscillate about the horizontal axis, and finally, spontaneously reverses its rotation about the vertical axis. Some rattlebacks can reverse direction of rotation many times, no matter what direction they were spun in initially.

In J Walker's paper, some other physics experiments involving rattlebacks are also described, and some rattleback models are presented. One of the models is shown in Fig. 1. It can be seen that rattlebacks have some dynamical asymmetry at the point of contact of the body with the plane.

A simple model of the rattleback (also described by J Walker) can be made by fixing a small rod to half of an egg, so that the rod makes a nonzero angle with the egg's axis of symmetry (Fig. 2). The motions that can be observed look very strange: press down on one end of the rod, and the egg, unexpectedly, will not wobble about the horizontal axis but will begin to spin slowly about the vertical axis; if we then press down on the other end of the rod, the egg will reverse the direction of spinning.

Here we are not going to delve deeply into the history of the subject, nor will we give an extensive narrative of the

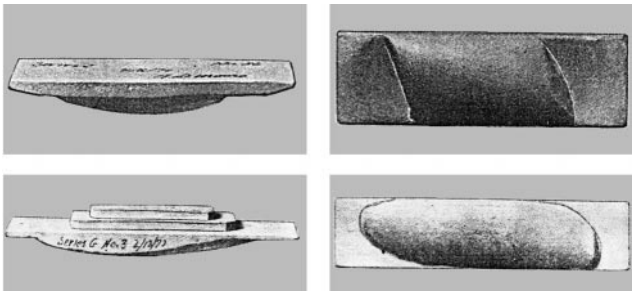

Figure 1. Two rattleback models from J Walker's paper [1].

A V Borisov, I S Mamaev Institute of Computer Science, Universitetskaya ul. 1, 426034 Izhevsk, Russian Federation
Tel. (7-3412) 76 82 95
E-mail: borisov@rcd.ru; mamaev@rcd.ru

Received 24 June 2002, revised 4 December 2002
Uspekhi Fizicheskikh Nauk **173** (4) 407 – 418 (2003)
Translated by S M Ramodanov; edited by A V Getling

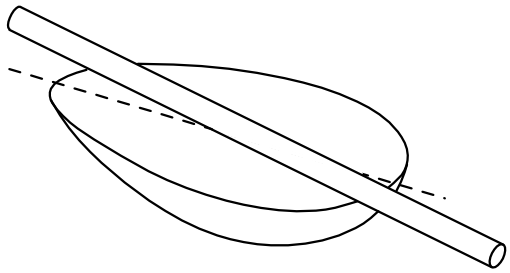

Figure 2. Another rattleback model from J Walker's paper [1].

rattleback's many other physical properties. For details see the references in Ref. [2]. Amazing features of the rattleback's dynamics were observed and described on an elementary physical level by G T Walker in 1895. We should also mention contributions by G Herglotz (1941) and C Magnus (1974), who mainly dealt with stability issues. Hereafter, we will reference Astapov [3], Karapetyan [4, 5], and Markeev [6], whose results are closely related to ours. We will also make reference to the numerical analysis performed by Lindberg and Longman [7] (a brief discussion of this work can be found in Section 5). Among other investigators of the problem, it is worth mentioning Kane and Levinson [9] and Pascal [10].

The rattleback is also called *the Celt* (*Celt Stone*). G T Walker noted that such unusual stones had been found by archaeologists in studying ancient Celtic features. Originally, the hatchet-shaped stones that exhibit the above-described unusual behavior after being set in motion on the surface of a table were named Celts.

There are several dynamical models for the rattleback. To perform a general analysis, one should consider the rattleback to be a heavy rigid body moving on a horizontal plane and subject to either dry (Coulomb) friction or viscous friction (proportional to the velocity). In this general statement, the problem is very complex and, therefore, a detailed qualitative analysis is impossible. At present, within the framework of this general approach, only a few series of numerical simulations have been performed.

A less realistic but more simple and demonstrative model for the rattleback can be based on nonholonomic mechanics (this will be referred to later as *the nonholonomic model*). Nonholonomic dynamical systems are situated in between the standard Lagrangian (and Hamiltonian) systems and the general dissipative systems. As a rule, in nonholonomic systems, an energy integral exists; thus they are conservative systems and, therefore, 'close' to Hamiltonian systems. On the other hand, nonholonomic systems lack an invariant measure [11] and, in this sense, they resemble dissipative systems (according to the Liouville theorem, any Hamiltonian system possesses a standard invariant measure).

A more detailed discussion of various forms of equations of nonholonomic mechanics is presented in Refs [2, 8, 12]. In this paper, however, we are not going to use these forms of equations but we will derive the equations of motion for the rattleback from the fundamental principles of dynamics (a balance of linear and angular momenta and some kinematics). Any nonholonomic system has at least one unintegrable constraint, and in our case this constraint implies that the point of contact of the body with the plane has zero velocity. Therefore, this nonholonomic model differs radically from the Hamiltonian model (with an absolutely smooth plane) and, at the same time, does not incorporate any sliding friction. Obviously, under the no-slip condition, the work done by the friction forces is zero and, therefore, the energy is conserved.

The nonholonomic model we develop adequately accommodates the main features of the rattleback's motion. Since there is no sliding and the energy is conserved, all the phenomena (wobbles, spin reversals) take longer time intervals than in actual practice. For an elementary description of the motion, however, this model has frequently been used [3 – 6, 8 – 10, 12].

2. Nonholonomic model. Equations of motion

As a model for the rattleback we consider here a heavy rigid body that rolls without slipping on a horizontal plane. The absence of sliding can be treated as a nonholonomic constraint placed on our system. This constraint simply means that the velocity of the point of contact is zero, that is,

$$\mathbf{v} + \boldsymbol{\omega} \times \mathbf{r} = 0\,, \tag{1}$$

where $\mathbf{r}$ is the position vector of the point of contact, Q, with respect to the center of mass, G; and $\mathbf{v}$ and $\boldsymbol{\omega}$ are the velocity of the center of mass and the angular velocity of the body (Fig. 3). In what follows, all vectors are assumed to refer to a body-fixed coordinate frame.

Using the balance of linear momentum and the balance of angular momentum relative to the point G (see Fig. 3), we get (with respect to the body-fixed frame) the following equations

$$\begin{aligned} &\frac{\mathrm{d}}{\mathrm{d}t}(m\mathbf{v}) = m\mathbf{v} \times \boldsymbol{\omega} - mg\boldsymbol{\gamma} + \mathbf{N}\,,\\ &\frac{\mathrm{d}}{\mathrm{d}t}(\mathbf{I}\boldsymbol{\omega}) = \mathbf{I}\boldsymbol{\omega} \times \boldsymbol{\omega} + \mathbf{r} \times \mathbf{N}\,. \end{aligned} \tag{2}$$

Here, $\mathbf{N}$ is the normal force acting on the body at the point of contact Q, $\boldsymbol{\gamma}$ is a unit vector pointing vertically upwards, m is the mass of the body, g is the acceleration due to gravity, and $\mathbf{I}$ is the inertia tensor referenced to the center of mass.

Using the constraint equation (1) and the first equation of (2), we eliminate $\mathbf{v}$ and $\mathbf{N}$ from (2) and, thus, obtain

$$\begin{aligned} &(\dot{\mathbf{I}\boldsymbol{\omega}}) + m\mathbf{r} \times (\dot{\boldsymbol{\omega}} \times \mathbf{r}) + m\mathbf{r} \times (\boldsymbol{\omega} \times \dot{\mathbf{r}})\\ &\qquad = \mathbf{I}\boldsymbol{\omega} \times \boldsymbol{\omega} + m(\boldsymbol{\omega}, \mathbf{r})\boldsymbol{\omega} \times \mathbf{r} + mg\mathbf{r} \times \boldsymbol{\gamma}\,. \end{aligned}$$

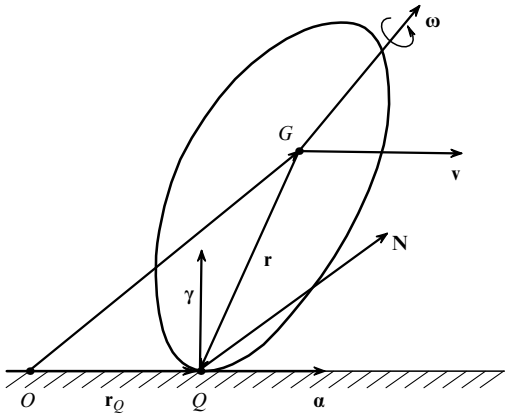

Figure 3. Rigid body on a plane.

The angular momentum of the body relative to the point of contact Q is

$$\mathbf{M} = \mathbf{I}\boldsymbol{\omega} + m\mathbf{r} \times (\boldsymbol{\omega} \times \mathbf{r}) . \tag{3}$$

Then, using the equations governing the behavior of the unit vector $\boldsymbol{\gamma}$ in the body-fixed frame, we represent the equations of motion in the form [8]

$$\begin{cases} \dot{\mathbf{M}} = \mathbf{M} \times \boldsymbol{\omega} + m\dot{\mathbf{r}} \times (\boldsymbol{\omega} \times \mathbf{r}) + mg\mathbf{r} \times \boldsymbol{\gamma} , \\ \dot{\boldsymbol{\gamma}} = \boldsymbol{\gamma} \times \boldsymbol{\omega} . \end{cases} \tag{4}$$

Here $\boldsymbol{\omega}$ should be expressed as a function of $\mathbf{M}$ with the use of (3).

Equations (4) are similar to the Euler–Poisson equations [13] governing the motion of a heavy rigid body fixed at one point. For equations (4), there exist two conserved quantities (first integrals):

$$\mathcal{H} = \frac{1}{2}(\mathbf{M}, \boldsymbol{\omega}) - mg(\mathbf{r}, \boldsymbol{\gamma}) , \qquad (\boldsymbol{\gamma}, \boldsymbol{\gamma}) = 1 . \tag{5}$$

The first one is the total energy of the system; the geometrical meaning of the second one is obvious. The vector $\boldsymbol{\gamma}$ is related to $\mathbf{r}$ by a Gaussian mapping

$$\boldsymbol{\gamma} = -\frac{\operatorname{grad} F(\mathbf{r})}{\left|\operatorname{grad} F(\mathbf{r})\right|} , \tag{6}$$

where $F(\mathbf{r}) = 0$ is the equation of the body's surface referring to a body-fixed frame.

Unlike the Euler–Poisson equations, an integral of areas and an invariant measure do not exist for equation (4) in the general case. This results in dynamical effects not typical for Hamiltonian systems [14].

3. Models for the body surface: a paraboloid and an ellipsoid

As an idealization, it is customary to assume that the surface of a rattleback is the surface of either an elliptic paraboloid or a three-axial ellipsoid.

The paraboloid model (the simpler one) is suitable for representation of the body's oscillations and rotation near the vertical (the point of contact coinciding with the paraboloid's vertex). This model, however, fails to describe the rolling motion of the body and its overturn. The equation of the body's surface and the Gaussian projection (6) are specified as follows:

$$\begin{aligned} &F(\mathbf{r}) = \frac{1}{2}\left(\frac{r_1^2}{a_1} + \frac{r_2^2}{a_2}\right) - (r_3 + h) = 0 , \\ &r_1 = -a_1\frac{\gamma_1}{\gamma_3} , \qquad r_2 = -a_2\frac{\gamma_2}{\gamma_3} , \\ &r_3 = -h + \frac{a_1\gamma_1^2 + a_2\gamma_3^2}{2\gamma_3^2} , \end{aligned} \tag{7}$$

where a_1 and a_2 are the principal radii of curvature at the paraboloid's vertex and h is the height of the center of mass situated at the axis of the paraboloid.

To study global effects (not only motions close to the rotation about the vertical), we consider the body to be a three-axial ellipsoid. The body's surface and the Gaussian projection are given by the equations

$$\begin{aligned} &F(\mathbf{r}) = \frac{r_1^2}{b_1^2} + \frac{r_2^2}{b_2^2} + \frac{r_3^2}{b_3^2} - 1 = 0 , \\ &r_i = \frac{b_i^2\gamma_i}{\sqrt{b_1^2\gamma_1^2 + b_2^2\gamma_2^2 + b_3^2\gamma_3^2}} , \end{aligned} \tag{8}$$

where b_1, b_2, and b_3 are the principal semiaxes of the ellipsoid. The principal radii of curvature, say, at the point $r_1 = r_2 = 0$, $r_3 = b_3$, are $a_1 = b_1^2/b_3$, $a_2 = b_2^2/b_3$.

Suppose that the center of mass is in both cases at the point $r_1 = r_2 = r_3 = 0$, and the principal axis of inertia OX_3 coincides with the principal geometric axis $\mathbf{e}_3$. *A distinguishing feature of rattlebacks is that the other two principal axes of inertia are rotated by an angle $\delta \neq 0$ relative to the other two principal geometric axes.* With respect to the principal geometric axes (not to the principal axes of inertia), the tensor of inertia has the form

$$\mathbf{I} = \begin{pmatrix} I_1\cos^2\delta + I_2\sin^2\delta & (I_1 - I_2)\cos\delta\sin\delta & 0 \\ (I_1 - I_2)\cos\delta\sin\delta & I_1\sin^2\delta + I_2\cos^2\delta & 0 \\ 0 & 0 & I_3 \end{pmatrix} , \tag{9}$$

where I_1, I_2, and I_3 are the principal moments of inertia at the center of mass.

4. Andoyaer–Deprit variables and three-dimensional Poincaré maps

In terms of the Euler angles, equations (4) describe the behavior of the nutation angle θ ($\cos\theta = \gamma_3$) and of the angle of proper rotation φ ($\tan\varphi = \gamma_1/\gamma_2$). These equations are exactly what we mainly deal with in the rest of the paper. We will keep in mind that, as soon as equations (4) are solved, the precession angle ψ and the motion of the point of contact can be obtained in quadratures [8, 13].

The Andoyaer–Deprit variables (L, G, H, l, g) are most convenient for a numerical analysis of the problem, and are used here instead of the Euler angles and the variables $(\mathbf{M}, \boldsymbol{\gamma})$. The physical meaning of the Andoyaer–Deprit variables is discussed, for example, in Ref. [13]. Here we give only the explicit conversion formulae

$$\begin{aligned} &M_1 = \sqrt{G^2 - L^2}\,\sin l , \quad M_2 = \sqrt{G^2 - L^2}\,\cos l , \quad M_3 = L , \\ &\gamma_1 = \left(\frac{H}{G}\sqrt{1 - \left(\frac{L}{G}\right)^2} + \frac{L}{G}\sqrt{1 - \left(\frac{H}{G}\right)^2}\,\cos g\right)\sin l \\ &\qquad + \sqrt{1 - \left(\frac{H}{G}\right)^2}\,\sin g\cos l , \\ &\gamma_2 = \left(\frac{H}{G}\sqrt{1 - \left(\frac{L}{G}\right)^2} + \frac{L}{G}\sqrt{1 - \left(\frac{H}{G}\right)^2}\,\cos g\right)\cos l \\ &\qquad - \sqrt{1 - \left(\frac{H}{G}\right)^2}\,\sin g\sin l , \\ &\gamma_3 = \left(\frac{H}{G}\right)\left(\frac{L}{G}\right) - \sqrt{1 - \left(\frac{L}{G}\right)^2}\sqrt{1 - \left(\frac{H}{G}\right)^2}\,\cos g . \end{aligned} \tag{10}$$

Once the two integrals of motion (5) are known, equations (4) specify a four-dimensional phase flow. We fix a three-dimensional hyperplane that intersects this flow and thereby

obtain a three-dimensional Poincaré map. It should be noted that, for the variables L, G, H, l, and g in (10), the equation $(\boldsymbol{\gamma}, \boldsymbol{\gamma}) = 1$ holds identically; therefore, given this integral, equations (10) specify a one-to-one transformation. Let the plane that intersects the four-dimensional level surface of energy $\mathcal{H}(L, G, H, l, g) = E$ be $g = g_0 = \text{const}$ and let $(l, L/G, H/G)$ be coordinates on this plane.

It should be emphasized that the classic Euler – Poincaré equations additionally have the integral of areas $H = \text{const}$. That is why the study of the behavior of solutions to these equations (as well as of any Hamiltonian system with two degrees of freedom) reduces to the analysis of a measure-preserving two-dimensional map.

In studying the rattleback dynamics, we face a much more complex situation, where the mapping is three-dimensional and does not generally preserve the measure. This complexity explains why the description of rattleback dynamics is not a trivial problem. Because of the absence of an invariant measure, our dynamical system is similar to a dissipative one, with complex attracting sets (strange attractors) appearing in the phase space. These sets are discussed below. The well-known Smale – Williams map serves as an example of a simple three-dimensional map with a chaotic attractor.

Thus, the analysis of the phase flow of equations (4) on an energy level reduces to the analysis of the mapping

$$\mathbf{x}_{n+1} = \mathcal{F}(\mathbf{x}_n), \qquad \mathbf{x}_n = \left(l, \frac{L}{G}, \frac{H}{G}\right). \tag{11}$$

Since $0 < l \leqslant 2\pi$, $-G \leqslant L \leqslant G$, *and* $-G \leqslant H \leqslant G$, *the map* (11) *is defined on some compact set*.

The fixed points of the mapping (11) correspond to periodic solutions to (4), the invariant curves of this mapping represent two-dimensional tori, and the two-dimensional invariant manifolds correspond to three-dimensional manifolds. Hereafter, we will use this terminology for both the flow and the mapping, hoping that no ambiguity will occur.

Comment. In view of (10), on any level surface $H/G = \text{const}$, the points with coordinates l and $l + 2\pi$ must be identified, and the straight line $L/G = 1$ is to be shrunk into a single point. Thus, the phase space of the mapping (11) is homeomorphic to $S^2 \times I$, where I is the segment $[-1, 1]$.

It is interesting to note that in our recently published book [8] (see also [15, 16]) a hierarchy of integrability was described for problems of nonholonomic dynamics. In this hierarchy, the rattleback dynamics is an extreme: the system is totally unintegrable, i.e., it has no additional tensor invariants. The opposite extreme is total integrability. In this case, the phase portrait of the mapping (11) is a family of invariant curves, and this map can thus be used to discover new integrable cases. A new integrable system found using this approach is described in Ref. [17] (see also [8]).

In Refs [15, 16, 18], we considered some systems with a limited set of tensor invariants — only one integral of motion or invariant measure. The most interesting one is the *Jacobi nonholonomic problem* [18] of the inertial rolling of a homogeneous solid sphere, whose center of mass moves over a three-axial ellipsoid. In this problem both an additional integral of motion and an invariant measure exist (hence there are no asymptotic solutions). However, this problem is not completely integrable except for the case of an ellipsoid of revolution first noticed by E Routh (see [16]). The phase portrait of the three-dimensional Poincaré map (11) is foliated into invariant surfaces, on which chaotic motion can be observed. This corresponds to the absence of another additional integral of motion necessary for complete integrability.

There are more examples of systems with a similar behavior of solutions, e.g., a dynamically asymmetric plate that rolls over a sphere and the rolling motion of an unbalanced Chaplygin's ball over a plane [16]. S A Chaplygin proved that the problem of rolling motion of a dynamically asymmetric, balanced ball over a horizontal plane without slipping is integrable (here, *dynamically asymmetric* means that the moments of inertia are arbitrary, and *balanced* implies that the center of mass coincides with the geometric center). In this problem, two integrals of motion and an invariant measure exist. In Ref. [15], we showed that if the center of mass does not coincide with the geometric center, the system lacks one integral and the invariant measure.

5. Symmetries of the flow and of the map

System (4) has some symmetry properties. We will consider them together with the corresponding symmetry properties of the mapping (11).

5.1 Reversibility

System (4) is invariant with respect to the change of variables (involution)

$$\boldsymbol{\gamma} \to \boldsymbol{\gamma}, \qquad \boldsymbol{\omega} \to -\boldsymbol{\omega}, \qquad t \to -t. \tag{12}$$

For the above-specified section $g_0 = 0$, this change of variables corresponds to the involution

$$l' = \pi - l, \quad \left(\frac{L}{G}\right)' = -\frac{L}{G}, \quad \left(\frac{H}{G}\right)' = -\frac{H}{G}, \quad \mathcal{F}' = \mathcal{F}^{-1},$$

where $\mathcal{F}^{-1}$ denotes the inverse of (11).

The following implications of the reversibility can be noted:

1. *In the neighborhood of the fixed points of the involution* (*near the equilibrium* $\boldsymbol{\omega} = 0$), *the KAM theory applies* [19]. A nonlinear analysis of the system's behavior in the vicinity of the stable equilibrium states was performed by A P Markeev [6] and will be discussed below.

2. *The fixed points of the mapping* $\mathcal{F}$ [*i.e., the periodic solutions of* (4)] *that are not fixed points of the involution* (12) *appear in pairs. Their multiplicators are equal in magnitude and opposite in sign.* The same is true in the case of any attractor. Thus, if the system (4) has an attracting set to which the solutions converge as $t \to +\infty$, then it also has an attracting set for $t \to -\infty$.

If the body has additional symmetry properties (geometric, dynamical), then other involutions may exist for the system (4).

5.2 Symmetry with respect to rotations of the axes

Suppose that the axis of symmetry $\mathbf{e}_3$ coincides with a principal axis of inertia (the other two axes of symmetry may be rotated by an angle δ relative to the other two axes of inertia); then equations (4) remain unchanged as the axes $\mathbf{e}_1$ and $\mathbf{e}_2$ are rotated by π about the axis $\mathbf{e}_3$, that is, they are invariant relative to the transformation

$$\begin{aligned} &\omega_1 \to -\omega_1, \qquad \omega_2 \to -\omega_2, \qquad \omega_3 \to \omega_3, \\ &\gamma_1 \to -\gamma_1, \qquad \gamma_2 \to -\gamma_2, \qquad \gamma_3 \to \gamma_3. \end{aligned} \tag{13}$$

For the map $\mathbf{x}_{n+1} = \mathcal{F}(\mathbf{x}_n)$, the symmetry

$$l' = l - \pi\,, \qquad \left(\frac{L}{G}\right)' = \frac{L}{G}\,, \qquad \left(\frac{H}{G}\right)' = \frac{H}{G}\,,$$

corresponds to this rotation.

Hence, *the map $\mathcal{F}$ is symmetric about the plane $l = \pi$,* and *all the fixed points that do not lie on this plane appear in pairs.*

5.3 Symmetry about a plane

Suppose that, for example, the axis of symmetry $\mathbf{e}_3$ coincides with a principal axis of inertia; then equations (4) are invariant with respect to the reflection about the plane $\mathbf{e}_1\mathbf{e}_2$ and the subsequent change of time, that is,

$$\omega_1 \to \omega_1\,, \qquad \omega_2 \to \omega_2\,, \qquad \omega_3 \to -\omega_3\,,$$

$$\gamma_1 \to \gamma_1\,, \qquad \gamma_2 \to \gamma_2\,, \qquad \gamma_3 \to -\gamma_3\,, \qquad t \to -t\,.$$

The three-dimensional map is invariant with respect to the involution $\mathcal{F}$:

$$l' = l\,, \qquad \left(\frac{L}{G}\right)' = -\left(\frac{L}{G}\right), \qquad \left(\frac{H}{G}\right)' = \frac{H}{G}\,, \qquad \mathcal{F}' = \mathcal{F}^{-1}. \tag{14}$$

Let us prove the following simple statement: *suppose that* (14) *holds true*; *then, for the fixed points of the map $\mathcal{F}$, one eigenvalue equals* 1 *and the product of the other two is also* 1.

Let us denote the matrix of the linear transformation (14) by $\sigma = \operatorname{diag}(1, -1, 1)$ and the linearization matrix for $\mathcal{F}$ in the neighborhood of a fixed point by $\mathbf{A}$. Then it follows from (14) that

$$\mathbf{A} = \sigma\mathbf{A}^{-1}\sigma\,,$$

and $\det\mathbf{A} = \det\mathbf{A}^{-1} = 1$, $a = \operatorname{Tr}\mathbf{A} = \operatorname{Tr}\mathbf{A}^{-1}$. The characteristic polynomial of $\mathbf{A}$ reads

$$\lambda^3 - a\lambda^2 + a\lambda - 1 = (\lambda - 1)(\lambda^2 + (1 - a)\lambda + 1)\,.$$

The fact that one of the eigenvalues equals unity indicates that the fixed points on the plane $L = 0$ are degenerate (see Figs 10 and 11). *If the other two multiplicators have zero imaginary parts, then closed invariant curves exist near these points.*

Similarly, we can discuss the case where all the principal axes of inertia coincide with axes of symmetry (see below). In this case, we have two additional planes of symmetry, and invariant curves exist in the vicinity of rotations about the vertical; these rotations are invariant when reflected in the planes containing the axis of rotation.

6. Known results in the dynamics of the rattleback

6.1 Stability of stationary rotation

Here we give an explicit form for the characteristic polynomial of system (4) linearized in the vicinity of a uniform rotation of the paraboloid about the vertical axis. This motion corresponds to a stationary solution $\boldsymbol{\omega} = (0, 0, \omega_0)$, $\boldsymbol{\gamma} = (0, 0, 1)$ of equation (4). The polynomial reads [3, 5]

$$\begin{aligned}
&\chi(\lambda) = \lambda^2(k_0\lambda^4 + k_1\lambda^3 + k_2\lambda^2 + k_3\lambda + k_4)\,,\\
&k_0 = (I_1 + mh^2)(I_2 + mh^2)\,,\\
&k_1 = \omega_0 mh(a_1 - a_2)I_{12}\,, \qquad k_3 = \omega_0^3 mh(a_1 - a_2)I_{12}\,,\\
&k_2 = \omega_0^2\big((I_3 - I_2)(I_3 - I_1) + mh\big((I_3 - I_{11})(a_2 - h)\\
&\quad + (I_3 - I_{22})(a_1 - h)\big) + m^2h^2(a_1 - h)(a_2 - h)\big)\\
&\quad + mg\big((I_{22} + mh^2)(a_2 - h) + (I_{11} + mh^2)(a_1 - h)\big)\,,\\
&k_4 = \omega_0^4\big((I_3 - I_2)(I_3 - I_1) + mh\big((I_3 - I_{11})(a_2 - h)\\
&\quad + (I_3 - I_{22})(a_1 - h)\big) + m^2h^2(a_1 - h)(a_2 - h)\big)\\
&\quad + \omega_0^2 mg\big((I_3 - I_{11})(a_2 - h) + (I_3 - I_{22})(a_1 - h)\\
&\quad + 2mh(a_1 - h)(a_2 - h)\big) + m^2g^2(a_1 - h)(a_2 - h)\,,
\end{aligned} \tag{15}$$

where I_{ij} are the components of the matrix (9). The linear stability of the rotation depends on the real parts of the roots of (15). For each value of the energy, there exist two rotational motions with frequencies ω_0 and $-\omega_0$.

Using the Routh–Hurwitz theorem, one can obtain the following conditions under which the rotation is stable.

Statement [3, 5]. *The rotational motion of a paraboloid about the vertical is stable if*

$$\begin{aligned}
&(1^\circ)\ \ (I_1 + I_2 + I_3)(a_1 + a_2 - 2h) -\\
&\qquad - mh\big(4h^2 - 3h(a_1 + a_2) + 2a_1a_2\big) = F_{\mathrm{GD}} > 0\,;\\
&(2^\circ)\ \ \omega_0 < -\omega_*\,, \quad \text{where} \quad \omega_*^2 = F_{\mathrm{GD}}^{-1}\, mg(a_1 - h)(a_2 - h)\,;
\end{aligned}$$

here F_{GD} is a 'geometrodynamical' function.

Let E_* be the energy value corresponding to ω_*.

This Lemma clearly shows that for $\delta \neq 0$ the stability of the rotation depends on its direction (clockwise or counterclockwise). *This fact discriminates nonholonomic systems from Hamiltonian systems.*

In addition, for the rotational motion to be stable the distribution of mass within the body must satisfy the condition $F_{\mathrm{GD}} > 0$, and the angular velocity must be sufficiently large. There exist bodies whose rotational motions in both directions are unstable.

In Fig. 4, graphs of the real parts of the eigenvalues are shown. In diagram (a), the 'geometrodynamical' condition (1°) is satisfied, while in diagram (b), condition (1°) is not satisfied.

These graphs indicate that, at energy values E for which $\omega_0 < \omega_*$, an unstable rotation about the vertical axis always exists, and the solutions tend to this motion as $t \to -\infty$. A typical phase portrait of the Poincaré map for a paraboloid ($E > E_*$) is shown in Fig. 5. All trajectories wind onto the stable, steady rotational motion for $t \to +\infty$ and on the unstable rotation for $t \to -\infty$. Simulations have shown that there are no other attractors in the phase space.

6.2 Hopf bifurcation. Birth of a cycle

In Ref. [5], it was shown that in the vicinity of the critical frequency, as the stability is lost ($\omega_0 > -\omega_*$, $\omega_0 \approx -\omega_*$), the Andronov–Hopf theorem on the birth of a cycle can be applied. In the vicinity of the rotation about a vertical axis, a stable limiting cycle arises. This cycle corresponds to a periodic solution of (4).

Figure 4a indicates that, for $\omega_0 < \omega_*$, $\omega_0 \approx \omega_*$ and with the direction of time reversed, the theorem on the birth of a

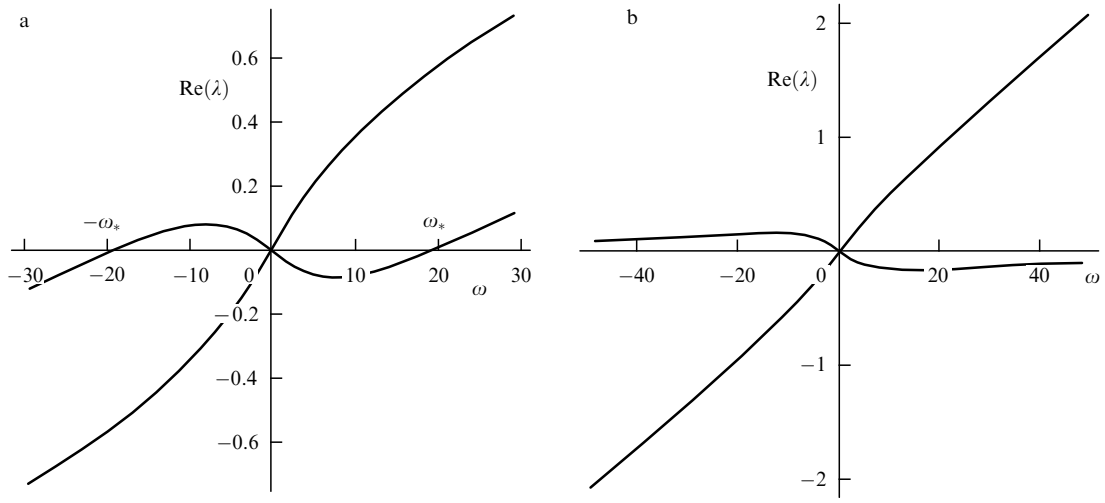

Figure 4. The real parts of the characteristic exponents for rotational motion about the vertical axis for different relations between the principal moments of inertia: (a) $I_1 = 5$, $I_2 = 6$, $I_3 = 7$, and condition (1°) is fulfilled; (b) $I_1 = 4$, $I_2 = 5$, $I_3 = 6$, and condition (1°) is not fulfilled ($m = 1$, $g = 100$, $a_1 = 9$, $a_2 = 4$, $h = 1$, $\delta = 0.2$).

cycle applies again. This is called *a reverse Hopf bifurcation* [the same result follows from the reversibility of (11)].

The results of simulations presented in Fig. 6 clearly show that, for $t \to +\infty$, in addition to the (stable) Karapetyan cycle, two other stable cycles appear (these two cycles persist as well when the physical parameters are slightly disturbed). The appearance of these additional cycles can hardly be predicted analytically. According to the reversibility property, near an unstable rotation about the vertical axis, similar unstable limiting cycles appear (the solutions are attracted by these cycles as $t \to -\infty$). There are no other attractors ($t \to \pm\infty$) in the phase space.

6.3 Nonlinear oscillations in the neighborhood of equilibrium

Some features of the rattleback's behavior were explained by A P Markeev. He studied small nonlinear oscillations in the neighborhood of equilibrium, i.e., at $\omega_0 = 0$ (this solution is a fixed point of involution). The characteristic polynomial (15) becomes biquadratic in this case and, for $a_1 > h$ and $a_2 > h$, it has two pairs of purely imaginary roots.

In Ref. [6], a normal form of equations (4) near the equilibrium was obtained up to third-order terms. It is as follows:

$$\begin{aligned} &\dot\rho_1 = -a\Omega_1^2\rho_1\rho_3\,, \qquad \dot\rho_2 = a\Omega_2^2\rho_2\rho_3\,, \\ &B\dot\rho_3 = a(\Omega_1^4\rho_1^2 - \Omega_2^4\rho_2^2)\,, \qquad \dot\sigma_1 = \Omega_1\,, \qquad \dot\sigma_2 = \Omega_2\,, \end{aligned} \tag{16}$$

where ρ_1, ρ_2, and ρ_3 are certain polar coordinates, σ_i are the angular coordinates; Ω_1 and Ω_2 are the frequencies of the normal oscillations; and $a, B = \text{const}$.

The equations for the unknowns ρ_1, ρ_2, and ρ_3 form a closed integrable system. Equations (16) have the following integrals:

$$\Omega_1^2\rho_1^2 + \Omega_2^2\rho_2^2 + B\rho_3^2 = \text{const}\,, \qquad \rho_1^\alpha\rho_2 = \text{const}\,, \qquad \alpha = \frac{\Omega_2^2}{\Omega_1^2}\,.$$

Using these quantities, a qualitative analysis of motion can be performed.

Comment. Explicit expressions for the coordinates ρ_i, σ_i and the frequencies Ω_i as functions of the phase variables and the first integrals of (4) can be found by solving the eigenvalue problem. These formulas are complex and can be found in Ref. [6].

The solutions to the equations in the normal form (16) are orbits on three-dimensional, invariant tori.

In addition, the normal form of the system (16) has a three-dimensional surface filled with doubly asymptotic trajectories. Physically, this means that the body rotating initially in one direction arrives for $t \to +\infty$ at the rotation in the reverse direction. Thus, in the vicinity of the equilibrium considered, the system (16) exhibits an almost Hamiltonian behavior [and, therefore, so does the system (4)].

Due to reversibility, the KAM theorem applies in the neighborhood of the equilibrium [19]; as an unperturbed system, one can take the normal form (16), and as a small parameter, the deviation of the energy from its minimum value $E_{\min} = mgh$.

Thus, *when the energy is small, three-dimensional Kolmogorov tori exist for the complete system* (4). In Fig. 9, three-dimensional cross sections of such tori, embedded into four-dimensional space, are illustrated.

The above considerations based on the KAM theory extend the results obtained by A P Markeev [6]. His results are of an asymptotic nature and remain valid only in finite time intervals.

6.4 Nonexistence of an invariant measure

This result is also a basis for understanding rattleback dynamics. It is valid for $\delta \neq 0$ and reflects the qualitative difference between the behavior of nonholonomic systems and that of Hamiltonian systems (according to the Liouville theorem, a Hamiltonian system has an invariant measure). As mentioned above, in this sense, nonholonomic systems are more similar to dissipative systems because in the phase space of a nonholonomic system attractors may occur.

Now we give a more rigorous formulation of the result [11].

Consider a paraboloid for which $I_1 \neq I_2$, $\delta \neq 0$ (as is the case for rattlebacks). In the vicinity of a rotation about the

vertical axis $\omega = \omega_0, \gamma_3 = 1, \omega_0 \neq 0$, *an invariant measure with analytic density does not exist*.

Comment. Assume that $\delta = 0$. This is true for paraboloids and ellipsoids (in particular, homogeneous) whose geometrical axes coincide with dynamical axes. It can be shown by direct calculation that, *near the rotation about a vertical axis, up to terms of arbitrarily high order, nothing prevents the existence of an invariant measure with analytic density*. Unfortunately, this measure has been obtained explicitly only in a few special cases. The form of this measure in the general case and the presence of other obstructions to its existence still calling for further investigation.

6.5 Numerical simulations by Lindberg and Longman

In addition to the analytical results discussed above, there are publications concerning computer simulations of the rattleback. Of special mention is a paper by Lindberg and Longman [7]. Their main result is as follows: suppose a paraboloid has been spun about the vertical in one direction; after a time, it passes the stage of wobbling and then starts rotating about the vertical again but in the reverse direction. For the values of the physical parameters used in Ref. [7], the condition (2°) of the stability of rotation about the vertical axis is not satisfied. More detailed investigations show that, for these values, a regular attractor (limiting cycle) occurs in the phase space. It should also be noted that the results presented in Ref. [7] are not completely verifiable. A more comprehensive discussion of these results can be found in Ref. [8].

7. Global dynamics of the rattleback. The strange attractor

Now we will describe the overall dynamics of the Poincaré map depending on the energy E. For $E > E_*$, the motion of the body approaches asymptotically a steady rotation, and for $E \lesssim E_*$, the Karapetyan cycle. At the same time, for small energies $E \gtrsim E_{\min}$, the system exhibits Hamiltonian properties, exactly as Markeev predicted. It will be shown below that, for energies in the range $[E_{\min}, E_*]$, the behavior of the system is chaotic: either intermittency phenomena can be observed or a strange attractor appears.

Next, we present the results of numerical simulations of the above-described three-dimensional map for various values of the energy. Two models, an ellipsoid and a paraboloid, are considered. The ellipsoid model is more complex because it admits overturns of the body.

For the simulations, we set the following dimensions (both for ellipsoid and paraboloid)

$$I_1 = 5\,, \quad I_2 = 6\,, \quad I_3 = 7\,, \quad m = 1\,, \quad g = 100\,; \qquad (17)$$

for the paraboloid (7) we assume $a_1 = 9, a_2 = 4, h = 1$ and for the ellipsoid, $b_1 = 3$, $b_2 = 2$, $b_3 = 1$. In both cases, the principal radii of curvature at the point $r_1 = r_2 = 0$, $r_3 = 1$ are equal; the stability is described by Fig. 4a, the critical value of the energy E_* is 1300, and the frequency of rotation about the vertical is $\omega_* = \pm 18.516\ldots$ Here, lengths are measured in centimeters, masses in kilograms, and times in $10^{-1/2}$ s.

7.1 Paraboloid model ($\delta = 0.2$)

A preliminary numerical analysis shows that the whole set of feasible energies $(E_{\min}, \infty)$, where $E_{\min} = mgh = 100$, can be divided into five regions within which the dynamics is similar for various E.

I. $E > E_*$. In the phase space, only rotation about the vertical in one direction is possible. This rotation is asymptotically stable (the map has a regular attractor; Fig. 5). Because of the reversibility, as $t \to -\infty$, the solutions tend to a steady rotation in the reverse direction. Note that the absolute values of the multiplicators of this stable rotation are less than unity, one of them being real and the other two forming a conjugate pair. Most likely, there is also an unstable limiting cycle on the one-dimensional separatrix originating from the unstable steady rotation. This cycle is a fixed point of the mapping (see Fig. 5).

II. $E_1 < E < E_*$, $933 < E_1 < 941$. As the energy becomes less than $E*$, the Andronov–Hopf bifurcation occurs (see Section 6). In the vicinity of the steady rotation about the vertical, which now becomes unstable, a limiting cycle forms (Fig. 6). Near the rotation in the reverse direction a reverse bifurcation occurs, and a limiting cycle also forms; it attracts solutions as $t \to -\infty$.

Moreover, a surprising feature takes place: two more limiting cycles, other than the Karapetyan cycle, form (see Fig. 6). This fact does not seem to be predictable analytically. A pair of similar cycles (stable as $t \to -\infty$) form near the unstable steady rotations. These cycles persist under a small perturbation of the parameters (17).

Here all trajectories unwind from the three unstable limiting cycles and wind onto the three stable ones. Two of them are direct extensions of the Karapetyan cycle to the given energy. The other four were found numerically by us. In the phase space, there are also unstable fixed points representing rotations about the vertical.

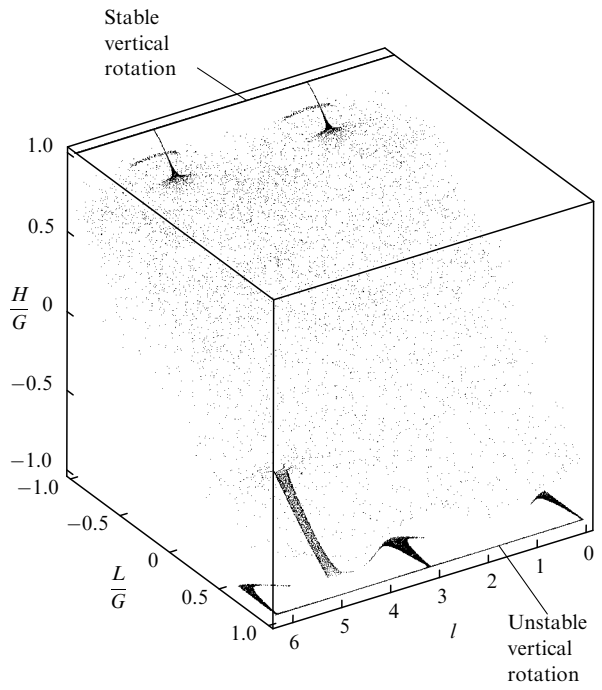

Figure 5. The case of $E = 2000$, $\delta = 0.005$, $g_0 = 0.5\pi$. Behavior for large values of energy $E > E_*$ is illustrated: all trajectories unwind from the unstable rotation about the vertical (as $t \to \infty$) and wind onto the stable rotation. (We assume here $\delta = 0.005$ to increase the time spent near the rotations about the vertical; this does not correspond to the value indicated in the text.)

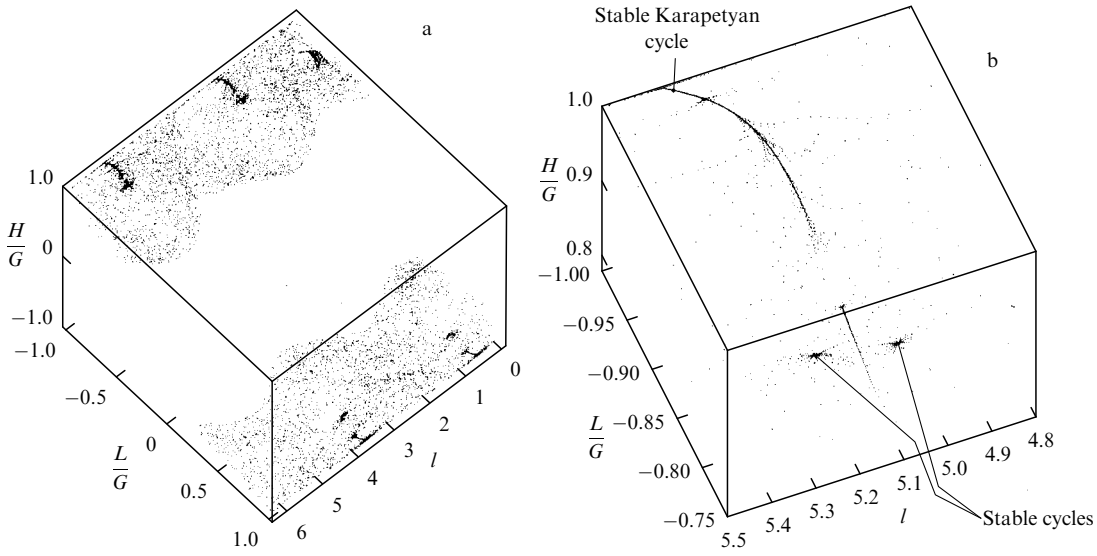

Figure 6. The case of $E = 1295 \lesssim 1300 = E_*$, $\delta = 0.2$, $g = 0.5\pi$. An outline of the phase portrait for an energy reduced to below E_*: all trajectories issue from the three unstable cycles (stable as $t \to \infty$) located at the lower right in diagram (a) and then wind onto the three stable cycles at the upper left in the figure (one of the cycles is the Karapetyan cycle). Diagram (b) illustrates the upper left part of diagram (a) on an enlarged scale.

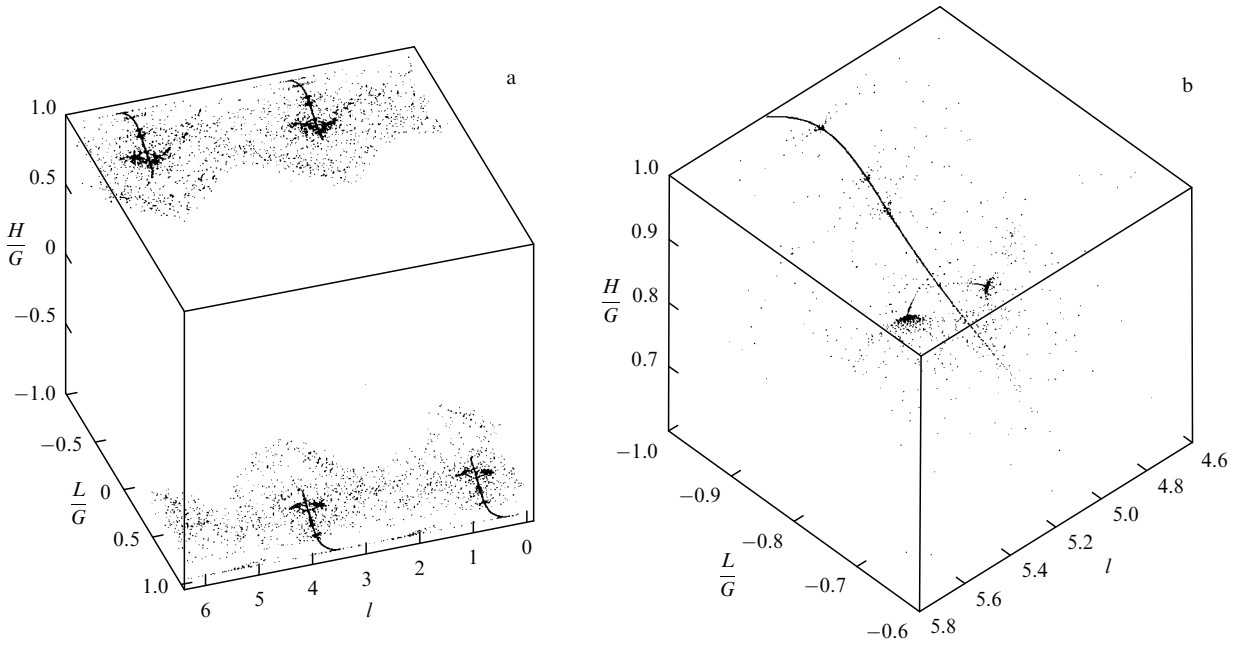

Figure 7. The case of $E = 900$, $\delta = 0.2$, $g = 0.5\pi$. An outline of the phase portrait after the loss of stability by the Karapetyan cycle. All trajectories unwind from the two unstable limiting cycles [at the bottom in diagram (a)] and wind onto the two stable cycles [the upper part of diagram (a)]. The region at the upper left in diagram (a) is shown on an enlarged scale in diagram (b).

III. $E_2 < E < E_1$, $560.7 < E_2 < 561.9$. As the energy passes through E_1, one of the Karapetyan cycles ceases to be stable, while the other two remain stable (Fig. 7). In the phase space, the regular attractors ($t \to \pm\infty$), which are two stable and two unstable limiting cycles, persist. The phase portrait also contains four unstable fixed points; two of them represent rotations about the vertical, and the other two are unstable Karapetyan cycles.

IV. $E_3 < E < E_2 - \varepsilon_1$, ε_1 being a small positive quantity. Formation of a strange attractor. Here, the two remaining limiting cycles become unstable, and an attracting set of a complex structure occurs (Fig. 8). Computations show that the maximal Lyapunov exponent for the trajectories of this set is positive. This set can thus be referred to as *a strange attractor*. The fact that such an attractor occurs in rattleback dynamics is unexpected and all the more remarkable because the initial system (4) is conservative. The physics behind the emergence of a strange attractor is that some limiting cycles cease to be stable; at the corresponding energy levels, the rattleback's behavior becomes globally chaotic. Note that, in the preceding regimes, some chaotic-oscillation stages were also observed; these oscillations, however, finally arrived at a

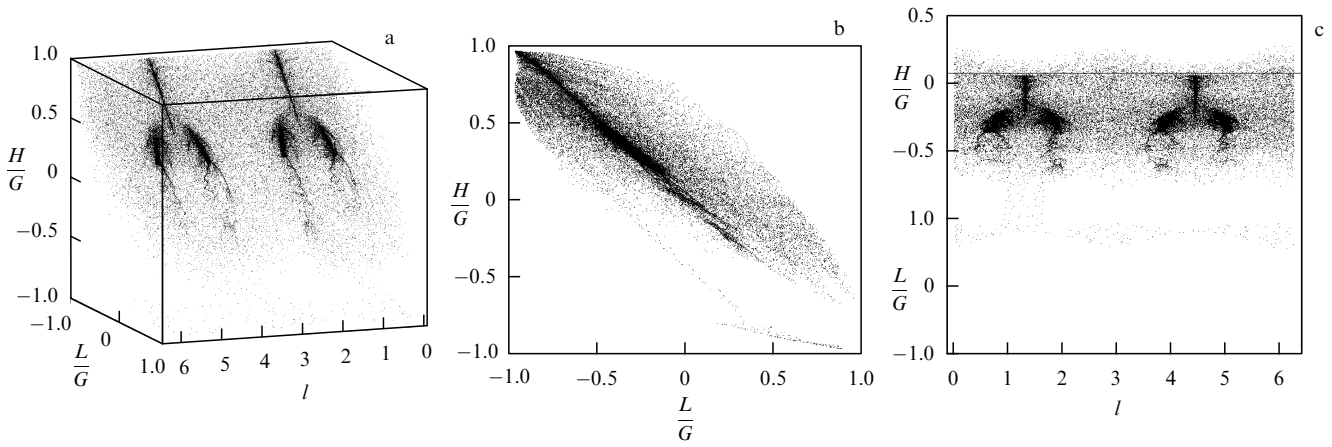

Figure 8. The case of $E = 555$, $\delta = 0.2$, $g = 0$. Birth of a strange attractor due to the loss of stability by the cycles. Panel (b) clearly shows that the trajectory leaves the neighborhood of steady rotation (at the bottom, near the straight line $L/G = H/G = -1$) and ends up in the complex attracting set — the strange attractor.

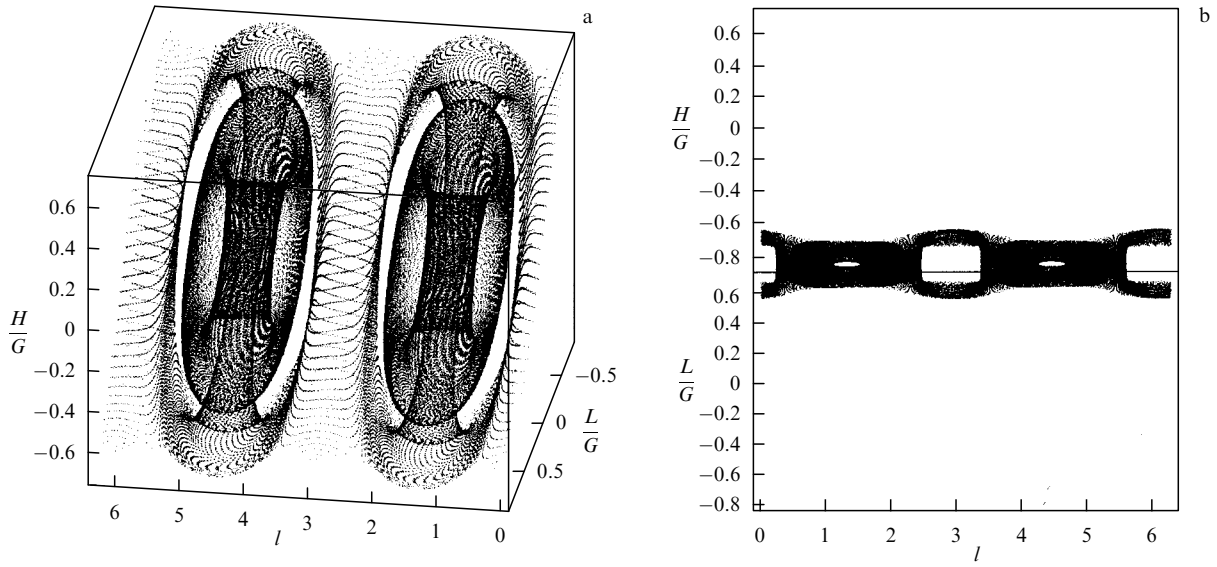

Figure 9. The case of $E = 200$, $\delta = 0.2$, $g_0 = 0$. An outline of the phase portrait for small energies viewed from various positions. Nonresonant persistent tori can clearly be seen.

regular periodic regime. As the energy is further decreased, other intricate, intermittent chaotic regimes occur. These regimes can hardly be studied even numerically.

V. $E_{\min} < E < E_{\min} + \varepsilon_2$, ε_2 being a small positive number. By this, we mean the neighborhood of the equilibrium state where small oscillations take place (the Markeev case; Fig. 9). As mentioned above, for small ε_2, three-dimensional, invariant Kolmogorov tori trapping other trajectories of the system are present here.

For $E_{\min} + \varepsilon_2 \leqslant E \leqslant E_3$, the behavior of the system has not yet been studied. A more detailed computer-aided analysis should focus on the behavior of the separatrices of fixed points and limiting cycles. The values of E_3 and ε_2 for which the strange attractor occurs should be estimated more accurately, and the attractor itself should get a more rigorous mathematical treatment.

7.2 Ellipsoid model

Here we will discuss some geometrical and dynamical features that distinguish the ellipsoid from the paraboloid.

I. The axes of symmetry coincide with the principal axes of inertia. Strictly speaking, this is not the case for rattlebacks. Below, we will consider slight perturbations of this configuration. Equations (4) are invariant under reflections about three mutually orthogonal planes. Hence, the periodic solutions (the fixed points of the mapping) lying in the planes (a) $L = 0$, (b) $l = 0$, and (c) $l = \pi/2, 3\pi/2$ are degenerate. They form curves in three-dimensional space, surrounded with invariant curves that correspond to two-dimensional tori of the phase flow (Fig. 10). Diffusion between these tori seems to be possible; however, its mechanism has not yet been studied. The curve that consists of fixed points represents oscillations of the ellipsoid about its principal axes (about horizontal axes in a fixed frame of reference). In this case, the absolute values of the multiplicators of rotations about the vertical axis equal unity.

II. The principal axes of inertia are rotated by an angle δ about the axis of symmetry $\mathbf{e}_3$. The periodic solutions in the plane $L = 0$ remain degenerate. The magnitudes of the multiplicators of the feasible rotations are no longer equal

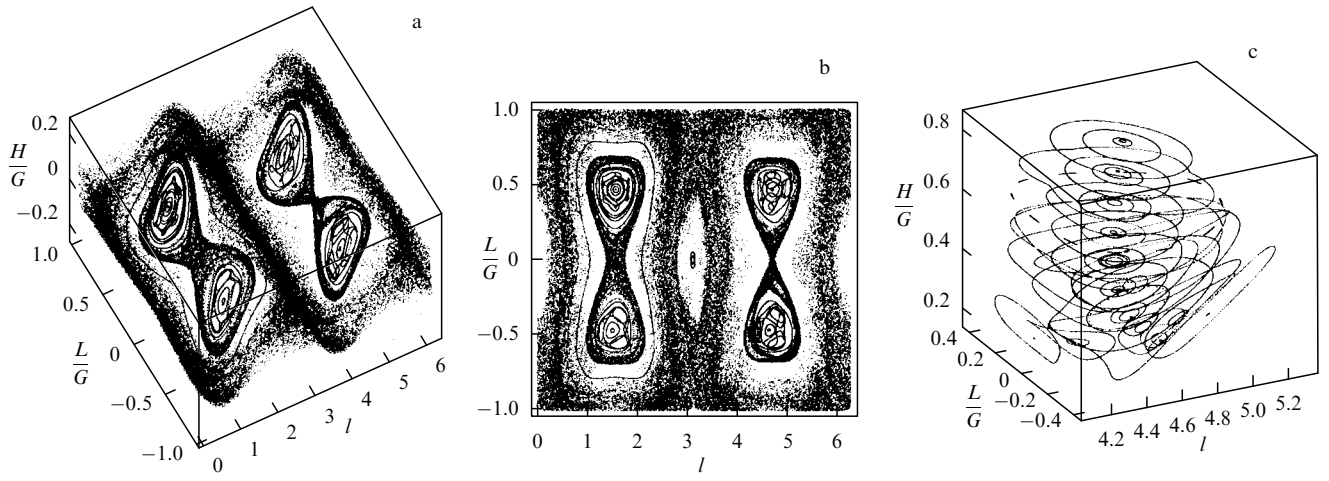

Figure 10. The phase portrait [viewed from various positions: panels (a) and (b)] for the case of an ellipsoid whose principal axes of inertia coincide with the axes of symmetry. The figure clearly shows the degeneration of periodic solutions caused by discrete symmetries. Panel (c) provides a magnified view of the phase portrait depicted in (a) and (b). The curve of degenerate periodic solutions together with persistent nearby one-dimensional invariant curves of the mapping are clearly seen. These invariant curves correspond to two-dimensional tori in the phase flow. One can notice that the tori do not trap other orbits ($E = 1500$).

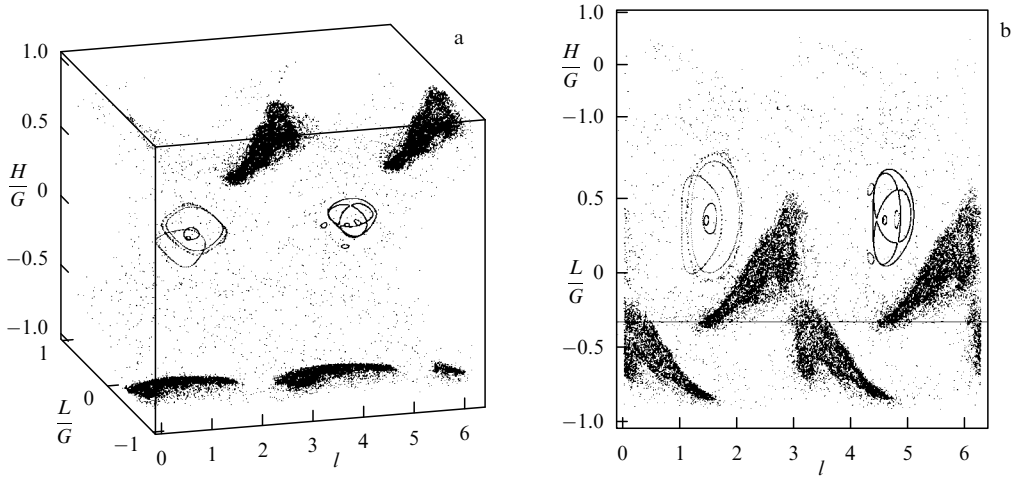

Figure 11. The phase portrait (viewed from various positions) for the case where only one principal axis of inertia is an axis of symmetry. Clearly seen are the shaded regions (strange attractors) attracting the solutions as $t \to +\infty$ (the upper part of the figure) and as $t \to -\infty$ (the lower part of the figure). In addition, one can notice persistent invariant curves near the degenerate periodic solutions ($E = 245$, $\theta = 0$, $\psi = 0.1$).

to unity. For $E > E_*$, one of rotations about $\mathbf{e}_3$ becomes stable. The birth of two attracting sets (for $t \to -\infty$ and $t \to +\infty$) is illustrated in Fig. 11. These sets are of the strange-attractor (or possibly quasi-attractor) type because their Lyapunov exponents are positive. Unlike the paraboloid case, not all trajectories converge to these attractors. There exists a region containing the above-described degenerate periodic solutions and two-dimensional invariant tori enclosing these solutions.

III. Arbitrary configuration of the axes. Let the dynamical axes $\mathbf{e}_1$ and $\mathbf{e}_2$ be rotated by an angle δ relative to the axis l_3, and let the axis $\mathbf{e}_3$ make an angle ζ with the corresponding axis of symmetry.

In this case, no geometric symmetries are present, and the fixed points that form the curve in Fig. 10b cease to be degenerate and become isolated. The results of simulations are as follows. In the phase space, consider a representative point that moves along a trajectory that has started near the elliptical fixed point of the unperturbed system (which corresponds to the coincidence of the geometrical and dynamical axes). Over a long time interval, this point remains close to the curve that is filled with degenerate fixed points in the unperturbed case (Fig. 12). It is easy to show that exponentially small effects come into play here; these effects are behind the existence of an almost invariant manifold containing perturbed trajectories. Note that the hyperbolic case is better explored, i.e., the case where a hyperbolic manifold exists in the unperturbed problem (e.g., a set consisting of points of the hyperbolic type), in contrast to the elliptic case shown in Fig. 10c. In accordance with the Hirsch – Pugh – Shub theorem, this hyperbolic manifold persists when the system is perturbed; however, the fixed points on this manifold either become isolated or even completely disappear.

In this case, the birth of strange attractors is also typical, and the global dynamics of the system is even less completely understood. It should be noted that, up to now, three-dimensional maps as such (both with and without an

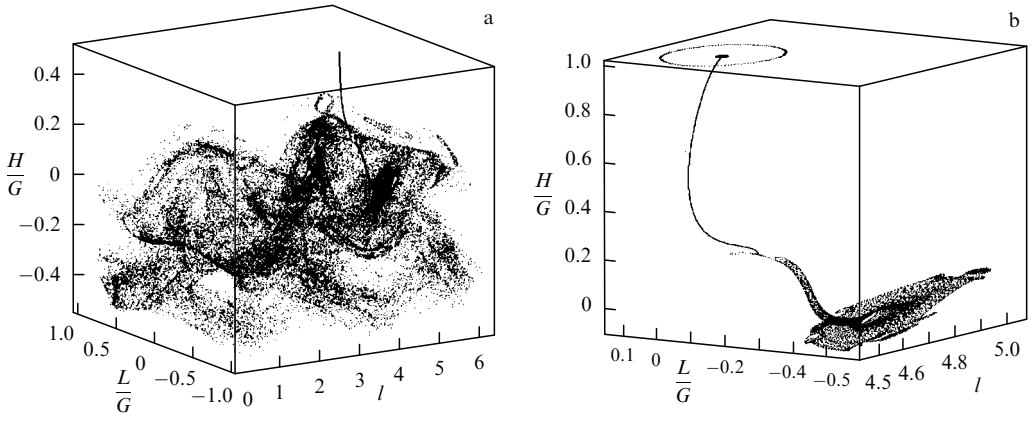

Figure 12. The phase portrait for the case where the dynamical axes are arbitrarily rotated relative to the axes of symmetry by a small angle ($\theta \neq 0, \psi \neq 0$, where θ, ψ, φ are the Euler angles describing the rotation of the axes of symmetry). It can be seen that the periodic solutions of the elliptic type cease to be degenerate. Panel (b) shows the initial fragments of the three curves from the previous portrait on an enlarged scale. The curve near which the solution with initial values $\theta = 0, \psi = 0$ (a periodic solution of the unperturbed system) finds itself over a long period of time is clearly seen ($E = 1500$, $\theta = 0.08$, $\psi = 0.01$, $\varphi = 0$).

invariant measure) have been investigated very little. The nonholonomic problems considered in this paper can serve as a testing area for new mathematical methods.

After this paper was submitted, the authors learned of an interesting work by H Broer, C Simó, and R Vitolo called "Bifurcations and strong attractors in the Lorentz-84 climate model with seasoned forcing" [20]. The paper deals with a nonautonomous model of the long-term climatic change in the atmosphere, suggested by Lorentz in 1984. The equations of this model are

$$\begin{cases} \dot{x} = -ax - y^2 - z^2 + aF\big(1 + \varepsilon\cos(\omega t)\big)\,, \\ \dot{y} = -y + xy - bxy + G\big(1 + \varepsilon\cos(\omega t)\big)\,, \\ \dot{z} = -z + bxy + xz\,, \\ a, b, \varepsilon, \omega = \text{const}\,, \end{cases} \tag{18}$$

where F and G are periodic functions with period $T = 2\pi/\omega$. The analysis of the equations reduces to the analysis of a three-dimensional mapping. Strange attractors were found for this system [20], and related scenarios of transitions to these attractors (destruction of invariant cycles) were discussed.

8. Conclusion

In this paper, some new properties of the rattleback's behavior discovered by numerical simulation are presented. These properties are closely related to the chaotic behavior of the system and the formation of strange attractors of three-dimensional maps. However, we have discussed here only a few aspects of the global dynamics of the rattleback. The global dynamics should be further explored in two aspects: general mathematical methods should be used more extensively (for example, to provide a more rigorous proof of the existence of strange attractors) and a physically more realistic model of the rattleback should be developed (it would he desirable to include the effects of dry and viscous friction, etc.).

The authors are grateful to V V Kozlov, A V Karapetyan, and D V Treshchev for their valuable comments.

References

1. Walker J *Sci. Am.* **241** (10) 144 (1979)
2. Markeev A P *Dinamika Tela, Soprikasayushchegosya s Tverdoĭ Poverkhnost'yu* (Dynamics of a Body Contacting a Rigid Surface) (Moscow: Nauka, 1992)
3. Astapov I S *Vestn. Mosk. Gos. Univ. Ser. 1 Mat., Mekh.* (2) 97 (1980) [*Mosc. Univ. Mech. Bull.* **35** 59 (1980)]
4. Karapetyan A V *Prikl. Mat. Mekh.* **45** (1) 42 (1981) [J. Appl. Math. Mech. **45** 30 (1982)]
5. Karapetyan A V *Izv. Akad. Nauk SSSR Mekh. Tverd. Tela* (2) 19 (1985)
6. Markeev A P *Prikl. Mat. Mekh.* **47** 575 (1983) [*J. Appl. Math. Mech.* **47** 473 (1984)]
7. Lindberg R E, Longman R W *Acta Mech.* **49** 81 (1983)
8. Borisov A V, Mamaev I S (Eds) *Negolonomnye Dinamicheskie Sistemy* (Nonholonomic Dynamical Systems) (Moscow–Izhevsk: Institut Komp'yuternykh Issledovaniĭ, 2002); http://ics.org.ru/cgi/getfile.cgi?id=22
9. Kane T R, Levinson D A *Int. J. Non-Linear Mech.* **17** 175 (1982)
10. Pascal M *Prikl. Mat. Mekh.* **47** 321 (1983)
11. Kozlov V V *Usp. Mekh.* **8** (3) 85 (1985)
12. Karapetyan A V *Ustoĭchivost' Statsionarnykh Dvizheniĭ* (Stability of Stationary Motions) (Moscow: Editorial URSS, 1998)
13. Borisov A V, Mamaev I S *Dinamika Tverdogo Tela* (Dynamics of the Rigid Body) (Moscow–Izhevsk: RKhD, 2001)
14. Borisov A V, Mamaev I S *Dokl. Ross. Akad. Nauk* **387** 764 (2002) [*Phys. Dokl.* **47** 892 (2002)]
15. Borisov A V, Mamaev I S *Reg. Chaot. Dyn.* **7** 177 (2002)
16. Borisov A V, Mamaev I S, Kilin A A *Reg. Chaot. Dyn.* **7** 201 (2002)
17. Borisov A V, Mamaev I S, Kilin A A *Prikl. Mat. Mekh.* (2003) (in preparation)
18. Borisov A V, Mamaev I S, Kilin A A *Dokl. Ross. Akad. Nauk* **385** 338 (2002) [*Phys. Dokl.* **47** 544 (2002)]
19. Sevryuk M B *Reversible Systems* (Lecture Notes in Mathematics, 1211) (Berlin: Springer-Verlag, 1986)
20. Broer H, Simó C, Vitolo R, Preprint No. 21 (Barcelona: UB-UPC Dynamical Systems Group, 2001); http://www.maia.ub.es/dsg/2001/index.html